Cell PRESS
Structure
Article

Structural Characterization of the Multidomain Regulatory Protein Rv1364c from *Mycobacterium tuberculosis*

Jack King-Scott,[1] Petr V. Konarev,[1] Santosh Panjikar,[1] Rositsa Jordanova,[1] Dmitri I. Svergun,[1] and Paul A. Tucker[1,*]
[1]EMBL Hamburg Outstation, c/o DESY, Notkestrasse 85, D22603, Hamburg, Germany
*Correspondence: tucker@embl-hamburg.de
DOI 10.1016/j.str.2010.11.010

SUMMARY

The open reading frame *rv1364c* of *Mycobacterium tuberculosis,* which regulates the stress-dependent σ factor, σ^F, has been analyzed structurally and functionally. Rv1364c contains domains with sequence similarity to the RsbP/RsbW/RsbV regulatory system of the stress-response σ factor of *Bacillus subtilis.* Rv1364c contains, sequentially, a PAS domain (which shows sequence similarity to the PAS domain of the *B. subtilis* RsbP protein), an active phosphatase domain, a kinase (anti-σ^F like) domain and a C-terminal anti-σ^F antagonist like domain. The crystal structures of two PAS domain constructs (at 2.3 and 1.6 Å) and a phosphatase/kinase dual domain construct (at 2.6 Å) are described. The PAS domain is shown to bind palmitic acid but to have 100 times greater affinity for palmitoleic acid. The full-length protein can exist in solution as both monomer and dimer. We speculate that a switch between monomer and dimer, possibly resulting from fatty acid binding, affects the accessibility of the serine of the C-terminal, anti-σ^F antagonist domain for dephosphorylation by the phosphatase domain thus indirectly altering the availability of σ^F.

INTRODUCTION

Bacteria can respond to stress conditions, such as starvation or other environmental challenges, by entering stationary phase. A major set of stress conditions, including temperature, oxygen, and osmotic stress, occurs when a human pathogenic bacterium first enters its host. To address the challenges, the pattern of gene expression must be changed and an efficient means of doing this is the use of alternate σ factors. σ factors provide promoter recognition for the RNA polymerase core enzyme, allowing open complex formation and transcription initiation, after which they dissociate. Since the regulons of a σ factor are extensive, they provide an effective mechanism for simultaneous regulation of many genes. Importantly, the availability of the alternate σ factors is regulated by anti-σ factors and anti-σ factor antagonists thus allowing a variety of signals to produce an extensive response.

The alternate σ factor, σ^B, of *Bacillus subtilis*, for which the regulatory genes are mainly in two adjacent operons, is one of the better understood systems (Benson and Haldenwang, 1992; Boylan et al., 1992). σ^B is bound, and thus inactivated, by the anti-σ factor RsbW, which is also a kinase for the anti-σ factor antagonist RsbV. RsbV can bind and sequester RsbW (thus releasing σ^B) when it is not phosphorylated. Phosphorylation disables RsbV binding to RsbW. The system is then regulated by ATP levels and two phosphatases, RsbP and RsbU, which act on RsbV and which pass on different, stress-related responses (Boylan et al., 1992; Benson and Haldenwang, 1993; Alper et al., 1996; Voelker et al., 1996). RsbP contains a PAS (Per-Arnt-Sim) domain at its N terminus as well as the phosphatase domain (Vijay et al., 2000). A second system regulating σ^B in *B. subtilis* is the RsbU/RsbT/RsbS system in which the anti-σ factor homolog, RsbT, binds RsbU and stimulates phosphatase activity. The anti-σ factor antagonist homolog, RsbS, part of the larger stressosome (Pané-Farré et al., 2005), binds RsbT only when it is not phosphorylated. It is the N-terminal domain of RsbU, which has an α-helical structure, that mediates the binding to RsbT (Hardwick et al., 2007).

Tuberculosis (TB) is a respiratory disease that has plagued mankind since antiquity. Since the last decade of the twentieth century, there have been indications of a steady increase in TB infections for a variety of reasons including poor health services, the growing HIV epidemic, and the development of drug-resistant forms of the tubercule bacillus *Mycobacterium tuberculosis* (Mtb), the causative agent of TB. Today, TB is recognized as one of the three major microbial killers and is responsible for 8–9 million new cases and between 1.5–2.5 million human deaths annually (Kaufmann and McMichael, 2005).

In Mtb the general stress response σ factor is σ^F (Rv3286c), but in this genome only the anti-σ factor (annotated RsbW, Rv3287c) is colocalized with σ^F. Two anti-σ^F factor antagonists, annotated as RsfA (Rv1365c) and RsfB (Rv3687c), have been identified (Malik et al., 2009). The protein with open reading frame Rv1364c is of especial interest in σ^F regulation and also, indirectly, σ^C regulation for five reasons. First it contains (based on sequence similarity) PAS and phosphatase domains (analogous to RsbP in *B. subtilis*), the kinase domain (analogous to the *B. subtilis* anti-σ factor RsbW), and the STAS (Sulphate Transporter and AntiSigma factor antagonist) domain (analogous to *B. subtilis* anti-σ factor antagonist RsbV). Second, yeast two-hybrid experiments on the full-length protein and on individual domains show interactions with σ^F and with other domains of Rv1364c (Parida et al., 2005). Third, Rv1364c is

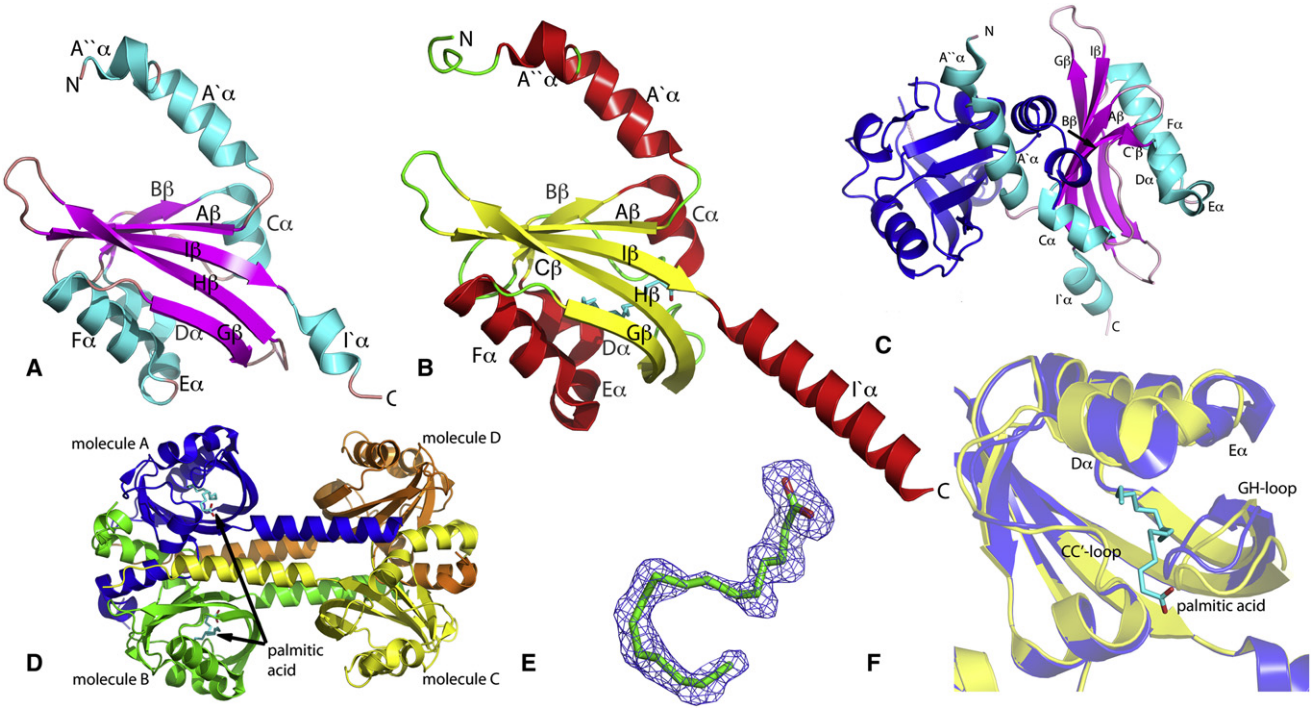

Figure 1. The PAS Domain Structure

(A) The Rv1364c$_{1-147}$ structure in cartoon representation with the α helices colored cyan and the β strands magenta. The secondary structure elements referred to in the text are labeled.

(B) The Rv1364c$_{1-156}$ structure in the same orientation with the α helices colored red and the β strands yellow. The palmitic acid in the binding cavity is shown in blue and red stick representation.

(C) A ribbon representation of the crystallographic dimer in the Rv1364c$^{1-147}$ structure, one molecule is colored as in (A) and the second (related by the symmetry operator 1-x,1-y, z) colored blue.

(D) A ribbon representation of the noncrystallographic tetramer in the Rv1364c1-156 structure . The two molecules on the left (blue and green) contain bound palmitic acid while those on the left do not.

(E) The electron density of the bound palmitic acid from a simulated annealing omit map contoured at three times the rms value of the map.

(F) An overlay of the major areas of difference between the molecules with (blue) and without (yellow) bound palmitic acid.

upregulated during starvation in Mtb (Betts et al., 2002) and the homolog in *M. bovis* (BCG) has been shown to be upregulated during intramacrophage survival (Li et al., 2004). Fourth, *rv1364c* is transcribed by two promoters, with the first, stronger, promoter being used under stress conditions (Li et al., 2004), and last the multidomain Rv1364c is present in pathogenic, slow-growing mycobacteria but not in the faster growing, nonpathogenic species such as *M. smegmatis* (Sachdeva et al., 2008) consistent with the absence of σ^F in that species (DeMaio et al., 1996, 1997). More recently (Greenstein et al., 2009) Rv1364c and its domains have been analyzed biochemically and the full-length protein investigated using small-angle X-ray scattering. It was shown that the C-terminal, STAS, domain can be phosphorylated by the kinase domain and dephosphorylated by the phosphatase domain with the kinase domain activating in some way the phosphatase domain in constructs containing both. In that work, the authors prefer to describe Rv1364c as related to the RsbU/RsbT/RsbS system because they demonstrate that the kinase domain (the equivalent of RsbT) activates the phosphatase.

In this paper, we describe the structures of two PAS domain constructs of Rv1364c and of a construct containing the kinase and phosphatase domains. We show that the PAS domain binds fatty acids and that the phosphatase domain is a manganese dependent PPM type phosphatase that is active both in the dual phosphatase/kinase construct and in the full-length molecule. We also describe low-resolution solution structures of monomeric and dimeric forms of the full-length protein.

RESULTS

The PAS Domain

The overall structures of the Rv1364c$_{1-147}$ (2.3 Å resolution with R_{cryst}/R_{free} of 24.5%/29.5%) and Rv1364c$_{1-156}$ (1.6 Å resolution with R_{cryst}/R_{free} of 18.2%/21.2%) constructs are very similar (Figure 1) with both exhibiting a typical α/β PAS fold (Taylor and Zhulin, 1999; Hefti et al., 2004). Using the nomenclature of (Gong et al., 1998), the PAS structure can be divided into five parts: (1) the N-terminal cap consisting of residues 5–26, which forms A''_α and A'_α; (2) the PAS core consisting of residues 27–70 forming the first three β sheets (A_β, B_β, and C_β) and three α helices (C_α, D_α, and E_α); (3) the helical connector, F_α, made up of residues 71–80; (4) the β scaffold containing residues 81–129, which contributes the remaining three anti-parallel β strands (G_β, H_β,

and I_β) of the central six-stranded β sheet; and (5) the C-terminal α helix, I'_α, made up of residues 130–138 (Figures 1A and 1B).

The asymmetric unit (ASU) of Rv1364c$_{1-147}$ contains one molecule; however, results from the PISA server (Krissinel and Henrick, 2007) suggest that the likely oligomeric state in solution would be a dimer (Figure 1C), in agreement with our size-exclusion chromatographic results. The resulting dimer is very similar to PAS dimers observed for DosH in *Escherichia coli* (PDB ID:1S66 [Park et al., 2004]), FixL from *Rhizobium melioti* (PDB ID:1D06 [Miyatake et al., 2000]), and NifL from *Azotobacter vinelandii* (PDB ID:2GJ3 [Key et al., 2007]). These dimeric structures all feature packing between the N-terminal helices and in the case of Rv1364c$_{1-147}$ and Rv1364c$_{1-156}$ these are A'α (Figures 1A–1D) . However PAS domains are typically linked to other domains and this dimerization interface is often not present in the full-length proteins.

The PAS Domain Binding Cavity

PAS domains form a large and diverse family of structurally homologous proteins which are often part of sensory systems, and which are known to bind a variety of effectors in their central cavity (for review and discussion, see Taylor and Zhulin, 1999; Vreede et al., 2003; Gilles-Gonzalez and Gonzalez, 2004). In Rv1364c this cavity is formed by the extended β sheet (formed by the β scaffold and the β strands from the PAS core) and by α helices: C_α, D_α, E_α, and F_α The cavity is lined by the residues I27, V29, L31, F38, Y45, F48, S49, A59, Y63, L66, I71, Y72, M74, L75, W90, L92, T94, Y96, R104, F106, F108, L125, V127, and D129. Whereas the cavities in Rv1364c$_{1-147}$, and those for molecules C and D in the Rv1364c$_{1-156}$ structure appear to be unoccupied, the cavities of molecules A and B of Rv1364c$_{1-156}$ are occupied by the fatty acid (FA) 1-hexyldecanoic acid (palmitic acid; C16:0). This was convincingly fitted into the electron density (Figure 1E) and refined. Palmitoleic acid also was modeled in the electron density; however, the FA did not fit as well as palmitic acid and could not be convincingly refined. Palmitic acid was subsequently identified over palmitoleic acid and others as being present in the protein solution by ESI-MS in negative ion mode.

The FA is completely enclosed by hydrophobic interactions with a single hydrogen bond between the carboxylate group and R104 (Figure 1D). This form of complete enclosure is common among fatty acid binding proteins (FABP) (Jones et al., 1988; Coe and Bernlohr, 1998; Sacchettini et al., 1989; Xu et al., 1993; Zanotti et al., 1992), although the curved FA conformation would appear to be less common. In Rv1364c the conformation appears to be stabilized by each end of the FA. The carboxylate end of C16:0 is anchored by hydrogen bonding to R104 while the C16 end is stabilized by hydrophobic contacts with F38, Y45, and Y63. The bend in the aliphatic chain appears to be generated by interactions of the methylene groups C7-C11 with the phenyl rings of F106 and F108.

A comparison of FA-bound molecules with those containing an empty cavity shows numerous small internal structural changes particularly in the CC' loop, D_α, E_α, and the GH loop (Figure 1F). The rmsd between 150 Ca atoms when superimposing (Krissinel and Henrick, 2004) molecules A and B (with bound FA), or C and D (without FA), is around 0.05 Å, whereas superimposing A and C (or B and D) the rmsd is 1.06 Å. Signaling in light and redox sensitive flavin-based PAS domains have been found to occur through the signal-dependent rearrangement of internal H-bonds (Genick et al., 1998). In Rv1364c, however, relatively few H-bonds are broken or formed when comparing the two forms. The overall effect of the structural changes appears to be a tightening of the binding cavity in the FA-bound form and the disappearance of an access hole visible in the surface of empty form. This access hole is determined by the separation between E_α and G_β that, in turn, is due to side-chain rearrangements of E65 and T94.

Table 1. The Binding Affinities of the FA Ligands to the Rv1364c$_{1-156}$ Construct

Fatty Acid	K_D[a] (nM)	ΔF_{max} (%)	n_H
Palmitic acid	400 ± 100	12.0 ± 1.9	1.12 ± 0.12
Palmitoleic acid	4.8 ± 0.90	13.0 ± 1.1	1.17 ± 0.08
Oleic acid	7.47 ± 1.29	10.0 ± 0.7	1.09 ± 0.08
Arachidonic acid	170 ± 20.0	6.9 ± 1.1	1.15 ± 0.01
Retinol	1020 ± 120	62.3 ± 4.5	1.18 ± 0.13

See also Figure S1.
[a] The K_D values were calculated from triplicate data points by nonlinear regression.

Fatty Acid Binding

Assuming that palmitic acid binding is an artifact resulting from expression of the PAS domain in *E. coli*, the fluorescent properties of the two tryptophan residues were used to screen the binding of various common FAs to the PAS domain. The binding affinities of palmitic acid (C16:0), palmitoleic acid (C16:1), oleic acid (C18:0), arachidonic acid (C20:4), and retinol were measured. The dissociation constant (K_D), the maximum fluorescence change upon saturation of the binding site (ΔF_{max}), and the Hill coefficient (n_H) from the fluorescent enhancement of the tryptophan residues at 345 nm are reported in Table 1. Prior to all measurements, any associated FA was removed by treatment of Rv1364c$_{1-156}$, with a LIPIDEX-1000 matrix.

Analysis of the fluorescence binding isotherms show the protein has only one binding site with all the ligands showing a Hill coefficient (n_H) of approximately 1 (Table 1). The binding affinities of the FA were determined to be in descending order: palmitoleic acid, oleic acid, arachidonic acid, palmitic acid, and retinol based upon the calculated K_D values. The binding affinity for palmitoleic and oleic acid (4.8 ± 0.9 and 7.5 ± 1.3 nM, respectively) are approximately two orders of magnitude greater than the other FAs. The binding curves for palmitic and palmitoleic acid are shown in Figure S1 (available online).

The Phosphatase/Kinase Dual Domain Structure

There are two molecules of Rv1364c$_{169-539}$ (2.6 Å resolution with R_{cryst}/R_{free} of 20.8%/26.7%) in the ASU. Apart from some residues at the N and C terminus of the construct, residues 215–216, 355–364, and 483–496 from molecule A and 355–364 and 483–496 from molecule B were not visible in the electron density and are not modeled. The final model contains four Mn^{2+} atoms within the ASU, two per molecule.

The structure (Figure 2A) shows the two central domains of Rv1364c, the N-terminal, phosphatase domain (Rv1364c$_{169-399}$)

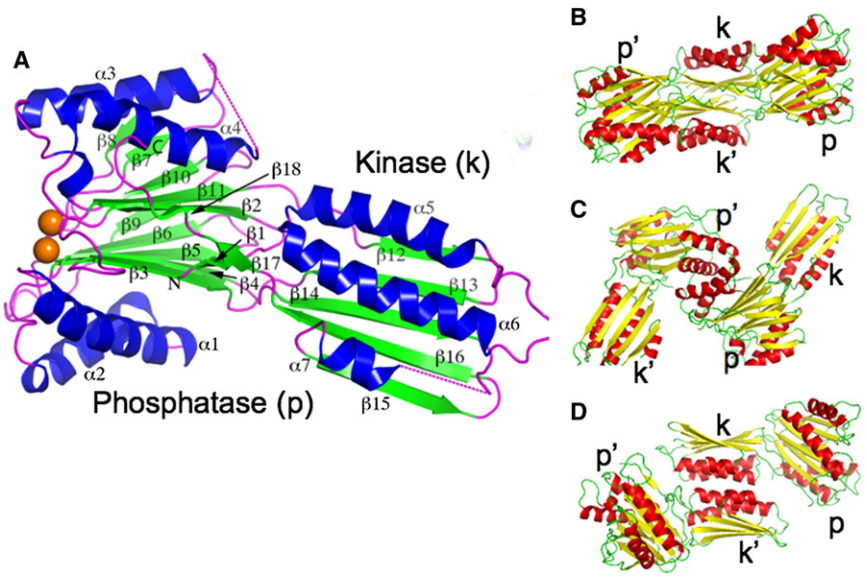

Figure 2. The Phosphatase-Kinase Dual Domain Structure

(A) A cartoon representation of the structure of the Rv1364c$_{169-539}$ dual domain with the α helices colored blue and the β strands green. The secondary structure elements as referred to in the text are labeled. The manganese ions of the phosphatase domain, on the left, are represented as tan spheres. The missing ATP binding flap, between β14 and α7 in the kinase domain, is indicated by a dashed line. The two domains are labeled.

(B–D) The three largest molecule-molecule interfaces observed in the crystal structure. In (B), the interaction is between kinase (k) domains. In (C), the interaction is between phosphatase (p) domains. In (D), the interface between kinase domains involves glycerol molecules and a sulfate ion and partly obscures the ATP binding pocket of the kinase domain.

and the C-terminal, kinase domain (Rv1364c$_{403-527}$). Rv1364c$_{169-399}$, previously classified by sequence similarity as a bacterial PPM phosphatase by the SMART server (Letunic et al., 2009; Schultz et al., 1998), contains the characteristic central ten-stranded β sandwich with two Mn^{2+} ions in the active site. Rv1364c$_{403-527}$ reveals no similarity to the Hanks-type serine kinases (Kennelly and Potts, 1996; Zhang, 1996) but is similar to the anti-σ factor from *Bacillus stearothermophilus* (Campbell et al., 2002). It consists of an α/β sandwich with a five-stranded β sheet and three α helices. The two domains are joined in a linear fashion by a linker (residues 400–403). The C-terminal tail (residues 527–535) forms an 11th β strand (β18, residues 527–532) alongside the Rv1364c$_{169-399}$ β sandwich. In the full-length protein this would connect to the C-terminal STAS domain. Prior to β18, a small two-stranded β sheet is formed between residues 171–173 from the N terminus (β1) and residues 525–527 from the C terminus (β17). This establishes a structural interaction between the two domains, although it is not clear from the structure alone how this might result in the kinase domain activating the phosphatase domain (Greenstein et al., 2009). The resulting interface created between the two domains buries a total surface area of 1000 Å^2 per domain. The two molecules in the ASU (Figure 2D) superimpose with an rmsd (root mean square displacement) of 0.51 Å (for 343 C$_\alpha$ atoms). The similarity of the two molecules despite the different crystal-packing environments suggests that the relative orientation of the two domains is fixed.

The Phosphatase Domain

The phosphatase domain (Figure 3A) is similar in structure to human phosphoprotein phosphatase 2C (PP2Cα [Barford et al., 1998]), PstP from Mtb (PDB ID:1TXO [Pullen et al., 2004], and 2CM1 [Wehenkel et al., 2007]), *Sa*STP from *Streptococcus agalactiae* (PDB ID:2PK0 [Rantanen et al., 2007]) and Ppm1k and Ppm1b from *Homo sapiens* (PDB ID:2IQ1 and 2P8E [Almo et al., 2007]). The protein sequences of all six proteins were aligned against the sequence from the Rv1364c$_{169-399}$ construct and the structures superimposed (Figures S2 and S4). The PPM family includes both prokaryotic and eukaryotic phosphatases (Cohen, 1994) that differ in size but maintain a common catalytic fold consisting of 9–11 signature motifs (1, 2, 3, 4, 5, 5a, 5b, 6, 7, 8, 9, 10, and 11). Eight of the motifs contain strictly conserved residues (motifs: 1[D], 2[D], 4[T], 5[G], 6[G], 8[DG], and 11[D]) (Shi et al., 1998; Zhang and Shi, 2004). Rv1364c, like other bacterial members of the PPM family (SpoIIE, RsbU, RsbX, and RsbP from *B. subtilis* and Icfg from *Synechocytsis* PCC) are completely missing motifs 5a and 5b (Shi et al., 1998; Bork et al., 1996). It would seem that all the PPM members missing these motifs are, or are thought to be, involved in σ factor regulation. All of the strictly conserved motifs are present in Rv1364c with three of them being involved in the formation of the PPM active site: D211(motif 1), D328(motif 8), and D387(motif 11). D211A and D328A mutations are known to abolish phosphatase activity in the full-length protein (Sachdeva et al., 2008). V212 the fourth and final residue from the phosphatase active site is positioned proximal to motif 1.

A superimposition of the Rv1364c$_{169-399}$ domain with the others (Figure 3B) confirms the structural similarity of the core domains. The 5a and 5b motifs, absent in Rv1364c, form a "flap" substructure between β8 and β9 in other PPM structures. As a result, β8 and β9, from Rv1364c$_{169-399}$, are significantly shorter and are joined by a long loop, which folds inward toward the α2/β5 loop. Other noticeable differences are (1) the length of α2 is approximately four residues shorter and consequently results in a shorter α1α2 loop; (2) the β2β3 loop exhibits a different orientation to that seen in the other structures folding outward from the active site where the equivalent loop in other structures is directed toward the α4β11 loop; (3) the β10α3 loop is 5 residues longer; and (7) as a consequence α3 is 7 residues longer (Figure 3B).

The Phosphatase Active Site

In the native crystal (see Experimental Procedures) the structure contains exactly two Mn^{2+} ions which are in the active site

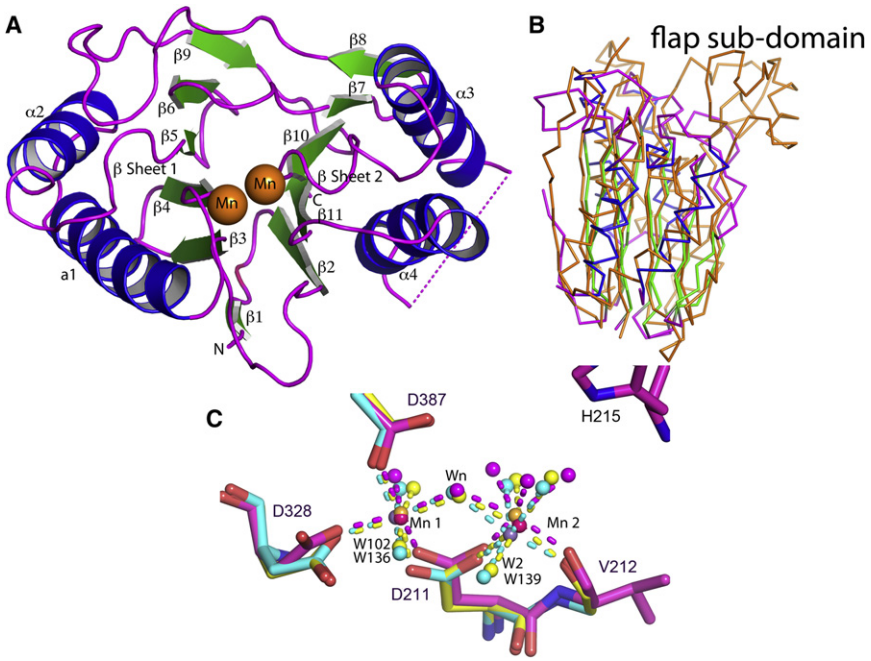

Figure 3. The Phosphatase Domain

(A) A ribbon representation of the phosphatase domain viewed looking into the phosphatase active site. The secondary structure elements are labeled. β1 forms a small two stranded β sheet with the C-terminal tail (residues 358–364) of the dual construct, which not shown in this figure. The Mn^{2+} ions in the active site are represented as brown spheres. The disordered α3-α4 loop is represented as a dashed line.

(B) An overlap of the Ca trace of different phosphatase domains. The crystal structure of the phosphatase domain of the dual domain crystal structure superimposed with 5 other known PPM phosphatase structures. Rv1364c (blue) is represented in as a Cα trace superimposed with PstP (green), PstP2 (cyan), Ppm1k (magenta), Ppm1b (yellow), PP2Cα (orange), and SaSTP (red).

(C) The superimposed active sites of the phosphatase domain (purple with Mn^{2+}atoms in brown), PP2Cα (yellow, PDB: 1A6Q with Mn^{2+} atoms in hot pink), and PstP2 (cyan, PDB: 2CM1 with Mn^{2+} atoms in deep purple). All water atoms are colored corresponding to the model's color. The presumed hydroxyl ion is labeled Wn.

See also Figures S2 and S4.

(Figure 3C) located at the top of the β sandwich. The crystals contained manganese as implied by the necessity of a divalent metal ion for crystallization and as confirmed by a fluorescent scan at the Mn K-edge. The active site bridges the two β sheets with three aspartic acids and one valine residue carbonyl coordinating the metals (Mn1 and Mn2) together with water molecules. The two metal ions are 3.8 Å apart, and are bridged by a hydroxyl ion (Wn). The metal-oxygen bond lengths range from 1.91–2.21 Å (Figure 3C).

The active site of PPM phosphatases is highly conserved as is evident when the active sites of PP2Cα (PDB ID: 1A6Q) (Das et al., 1996) and Pstp2 (PDB ID: 2CM1) (Wehenkel et al., 2007) are superimposed upon the active site of $Rv1364c_{169-399}$ (Figure 3C). The metal-residue bonds and angles are similar for all three active sites but due to the relatively low resolution of the structure reported here the metal coordination spheres probably do not have their full complement of water molecules. The hydoxyl ion (Wn in Figure 3C) is proposed to be responsible for the hydrolysis of the phosphoester bond in the active phosphatase. It is thought to act as a nucleophile, attacking the phosphorous atom in an S_N2 mechanism (Das et al., 1996).

Phosphatase Activity Assays

PPM phosphatases are known to be dependent on Mg^{2+} or Mn^{2+} ions for activity toward phosphothreonines or phosphoserines (Bork et al., 1996). The nonspecific substrate *para*-nitrophenyl phosphate was used in a colorimetric assay to quantitatively measure the activity of the phosphatase domain. As for the *B. subtilis* homolog, SpoIEE, the $Rv1364c_{169-539}$ construct is, as previously shown (Sachdeva et al., 2008), solely dependent on Mn^{2+}, with Mg^{2+} alone resulting in inactive phosphatase. The assay was also used to show that the dimeric fraction of the full-length protein, Rv1364c, is approximately twice as active as the dual-domain construct ($Rv1364c_{169-539}$) used for the structural work. Compared to other characterized PPM phosphatases, $Rv1364c_{169-539}$ appears to show low activity. Both constructs show Michaelis-Menten kinetics. The results are summarized in Table 2 and further details given in Figure S3.

The difference in phosphatase activity between the dual construct and the full-length protein is significant and could arise from differences in the availability of the phosphatase domain, which would be much less evident for the small artificial substrate used rather than the real substrate. The general acid, which is thought to protonate the leaving group, has been identified through mutagenesis experiments, pH-rate profiles, and by Brönsted analysis (Jackson et al., 2003) in PP2Cα as H62. The sequence surrounding H62 in PP2Cα, 60-DGH-62 differs in prokaryotic PPM family members, which frequently have a 3 residue insert preceding the histidine residue. In PstP, the conserved histidine is H43 and is preceded by the insert 38-DGMGGH-43. Consequently H43 is 7.2 Å away from Wn (Pullen et al., 2004). Since no other functional equivalent is nearby it is thought that a water molecule may act as a general acid for the reaction instead. In $Rv1364c_{169-399}$, H215 is a good

Table 2. Characterization of the Phosphatase Activity for the Dual Phosphatase/Kinase Domain and Full-Length Rv1364c with the Artificial Substrate *p*NPP

Phosphatase Construct	Substrate	V_{max}[a] ($\mu mols \cdot min^{-1} \cdot mg^{-1}$)	K_m (mM)
Rv1364c	*p*NPP	0.02 ± 0.001	31.2 ± 6.3
Phosphatase/ kinase domain	*p*NPP	0.008 ± 0.0004	26.2 ± 3.6

See also Figure S3.

[a] Enzyme reactions were performed with various concentrations of *p*NPP according to the method of Babson and Phillips (1966). The V_{max} and K_m values were calculated from duplicates by nonlinear regression.

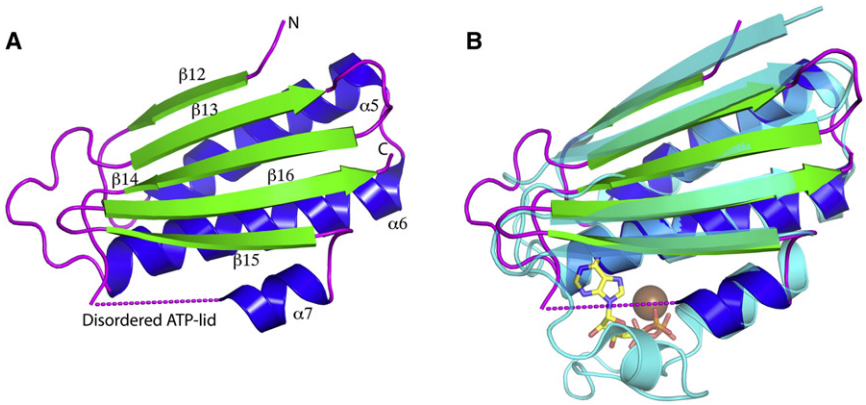

Figure 4. The Kinase Domain

(A) A ribbon representation of the kinase domain showing the disordered ATP lid by a dashed line. α helices are blue, β strands are green, and loops are pink.

(B) For comparison the kinase domain of the anti-σ factor SpoIIAB from *Bacillus stearothermophilus* (PDB ID:1TID, Masuda et al., 2004) is overlayed in cyan. The superimposed structure displays the ATP lid with ATP in stick form and Mg2+ as a brown sphere.

See also Figure S4.

candidate for the general acid. H215 is closer to the hydroxyl (Wn) than in the PstP structure perhaps because there is only a 2 residue insert in the sequence, 211-DVVGH-215.

The Kinase Domain

The structure of the Rv1364c$_{403-527}$ domain displays a typical Bergerat fold (Bergerat et al., 1997) common to sensor kinases (SK) (Duncan and Losick, 1993; Min et al., 1993) and ATPases of the GHKL superfamily (Dutta and Inouye, 2000). As in the SpoIIAB structure, the Rv1364c$_{403-527}$ domain lacks the H-box common to SKs, but it does contain the conserved N, G1, G2, and G3 boxes (Min et al., 1993). The structure is an α/β sandwich consisting of a four-stranded anti-parallel β sheet and three α helices (β12, α5, α6, β13, β14, α7, β15, and β16) (Figure 4A). Like the SpoIIAB structure (Campbell et al., 2002) Rv1364c$_{403-527}$ has an additional N-terminal β strand and α helix, β12 and α5. Although these additional secondary structural elements have been demonstrated to be involved in the dimerization of SpoIIAB, there is no evidence that they have a similar role for Rv1364c. The ATP-binding site of a Bergerat fold is located in a deep pocket between the three α helices and is backed by the β sheet. Both kinase domains in the ASU are nearly identical (rmsd = 0.22 Å for 112 superimposed C_α atoms) and both copies have a disordered ATP-binding lid (residues 483–496). Despite this disorder, a number of key residues that would interact directly or indirectly with ATP are still clearly defined. These residues are all positioned in the highly conserved GHKL boxes suggesting that Rv1364c would bind ATP in a similar manner. The crystal structure of SpoIIAB with ATP and Mg^{2+} bound (PDB ID: 1TID [Masuda et al., 2004]) when superimposed, using the SSM algorithm (Krissinel and Henrick, 2004), on the Rv1364c$_{403-527}$ (kinase) domain structure yields an rmsd of 1.09 Å for 84 C_α atoms (Figure 4B).

In the SpoIIAB structure, the N-box contains an absolutely conserved asparagine residue, which directly coordinates with the Mg^{2+} ion and is thought to be essential for the ATPase and kinase activity of GHKL super family members (Ban et al., 1999; Bilwes et al., 2001; Prodromou et al., 1997; Wigley et al., 1991). N448 is the equivalent asparagine residue in Rv1364c$_{403-527}$. Another key catalytic residue believed to be the catalytic base that promotes the nucleophilic attack by a water molecule on ATP (Jackson et al., 2003) is E444 in Rv1364c$_{403-527}$. It is positioned near the N-box and is conserved in GHKL ATPases, but not in SKs. The role of this aspartate is similar to that of the strictly conserved aspartate residue in the HANKS-type S/T/Y kinases (Taylor and Radzio-Andzelm, 1994; Yoon and Cook, 1987). H452, a conserved N-box residue appears, using the structural superposition of Figure 4B, to be in a position to stabilize the β-phosphate of an ATP molecule (Campbell et al., 2002). Further support for this hypothesis is obtained comparing the structure of the Rv1364c$_{403-527}$ domain with the SpoIIAB and CheA structures. E444K, N448K, and H452A mutations have been shown to eliminate kinase activity (Greenstein et al., 2009).

The G1-, G2-, and G3-boxes are so named because of the strict conservation of glycine residues in these motifs. G1 and G2, flank the ATP-lid where they are thought to act as hinges (Dutta and Inouye, 2000). Other residues found in these motifs are also involved in direct binding of an ATP molecule, for example D480 in G1 and T517 in G3 are conserved. However, there are notable differences (comparative sequence alignments are given in Figure S4); in particular, the normally conserved glycine in G1 is a tryptophan in Rv1364c and the ATP-lid is significantly shorter than in other GHKL family members.

The work of Sachdeva et al. (2008), suggested that the kinase domain of Rv1364c had, at best, limited ATPase activity. Although this observation would be of fundamental importance to understanding the function of this gene product in pathogenic mycobacteria, more recent work (Greenstein et al., 2009) would suggest that the kinase domain is active if the Mg^{2+} concentration is kept at physiological levels. Our own assays (data not shown) confirm ATPase activity.

Oligomeric State of the Phosphatase-Kinase Construct

Rv1364c$_{169-539}$ elutes from a gel filtration column as both monomer and dimer. The nature of the dimer interface in solution is not clear from the crystal structure (Figures 2B–2D show the three principle interfaces found in the crystal lattice) at least, in part, because a sulfate ion and a glycerol molecule are involved in the formation of crystal contacts shown in Figure 2D. A more comprehensive discussion of dimer interfaces in the crystal is given in Supplemental Information and is used further in the solution scattering work described there and below.

Table 3. Analysis of the Monomeric and Dimeric Samples of Rv1364c by Small-Angle X-ray Scattering

Sample	C, mg/ml	R_g, nm	D_{max}, nm	MM_{exp}, kDa	V_p, nm^3
Monomer	1.0, 2.0, 4.1	3.88 ± 0.05	14.0 ± 1.0	64 ± 5	142 ± 10
Dimer	1.7, 3.4, 6.7	5.22 ± 0.07	17.0 ± 1.0	123 ± 10	289 ± 20

C, solute concentration; R_g, radius of gyration; D_{max}, maximum size of the particle; V_p, excluded volume of the hydrated particle, estimated from ab initio models (DAMMIN/GASBOR).

Rv1364c Solution Studies

Size exclusion experiments indicate that the full-length protein, like the phosphatase-kinase dual construct, can exist as monomers and dimers in solution. In the case of the full-length protein, it would appear that there is an activation barrier to monomer-dimer conversion since they could be isolated separately. Small-angle X-ray scattering (SAXS) was used to further investigate the two different oligomeric species of the protein isolated from size exclusion chromatography. Rv1364c was analyzed in solution as both a monomer at between 1.0 and 4.1 mg/ml and as dimer at concentrations between 1.7 and 6.7 mg/ml. The overall parameters of the solutes (R_g , D_{max}, MM_{exp}, and V_p in Table 3) were estimated for both species. Multiple runs of the programs GASBOR/DAMMIN (Svergun, 1999; Svergun et al., 2001) were used to produce an averaged ab initio model for both the monomeric and dimeric species (Figures 5A and 5C). Good fits to the scattering data (Figure S5) were obtained with discrepancies ("χ") of 1.08 and 1.21, respectively. The overall shape, as shown by the models and suggested by the asymmetric tail in the distance distribution function ($p(r)$, in Figure S5), is an elongated shape for both states.

Several runs of the program BUNCH using the two crystal structures ($Rv1364c_{1\text{-}156}$ and $Rv1364c_{169\text{-}539}$) and a homology model of the C-terminal STAS domain, $Rv1364c_{559\text{-}653}$, as rigid bodies, produced a good model for the monomeric species (χ = 2.10). The BUNCH derived model show a good fit to the ab initio envelope (Figures 5A and 5B) but exhibits some small discrepancies when compared with the scattering data probably indicating some flexibility in the real monomer which is most likely due to the 28 residue linker between the first three domains and the C-terminal domain of the protein. The ab initio envelope of the dimer (from DAMMIN) with (χ = 1.22) and without (χ = 1.21) the imposition of 2-fold symmetry is shown in Figure 5C. Fits of a dimer (using BUNCH) without restraints is shown in Figure 5D (χ = 2.23) with the ab initio model superimposed in Figure 5E. It is not possible to say if one of the dimer interfaces of the dual domain is a determinant of the dimer in solution, but the favored one of the possibilities is described in the Supplemental Information where it is also explained that this could affect access to the phosphatase active site. The dimensions and the overall parameters of the Rv1364c ab initio dimer models correlate well with SAXS envelopes obtained by Greenstein et al. (2009), for comparison several individual ab initio models obtained with the imposition of 2-fold symmetry are shown in Figure S5. We also investigated whether or not dimeric models, where the phosphatase and kinase domains were allowed to move independently, would give improved fits. The fits are necessarily slightly better (data not shown), since there are more degrees of freedom, but they are not significantly so.

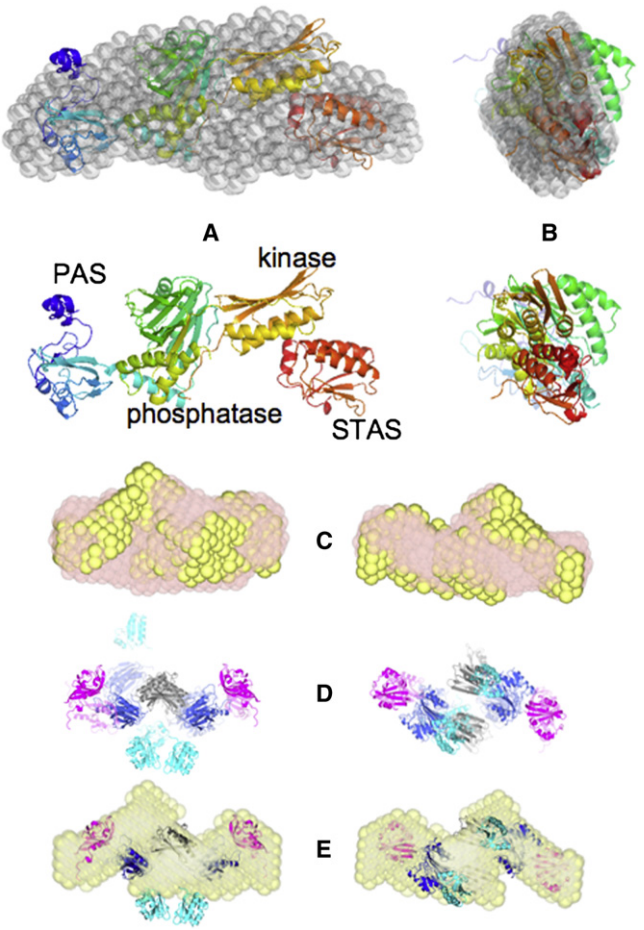

Figure 5. Solution Structures of Full-Length Rv1364c

(A) The SAXS determined ab initio envelope of the Rv1364c monomer in transparent gray superimposed on the BUNCH determined fit of the separate domains to the scattering data. The four domains are indicated. The PAS domain spans the colors from blue to cyan, the phosphatase domain from cyan to yellow, the kinase domain from yellow to orange and the STAS domain from orange to red.

(B) As in (A) but rotated 90° about the vertical axis.

(C) The ab initio envelope of the dimer with (yellow) and without (semitransparent tan) the application of 2-fold symmetry.

(D) BUNCH-derived dimer models obtained without restraints with (full colors) and without (semitransparent colors) 2-fold symmetry. The PAS domains are colored violet, the phosphatase domains blue, the kinase domains gray and the STAS domains cyan.

(E) Ab initio envelope (semitransparent yellow) superimposed on the BUNCH dimer model with 2-fold symmetry. Panels (C)–(E) show two views rotated 90° about the horizontal axis.

See also Movie S1 and Figure S5.

DISCUSSION

To date, mycobacteria have not been demonstrated to have an equivalent of the *B. subtilis* stressosome. It is probably therefore dangerous to draw too close parallels between the domains of Rv1364c and potential *B. subtilis* homologs. To be more specific,

on the one hand the N terminus of Rv1364c is structurally like the RsbP protein of *B. subtilis*, thus suggesting it is similar to the downstream RsbP/RsbV/RsbW regulatory system. On the other hand, the activation of the Rv1364c phosphatase by the kinase domain is more similar to the mode of action of the more upstream regulation involving the RsbU/RsbT/RsbS system (Greenstein et al., 2009).

We suspect that, based on the existence and structure of the N-terminal PAS domain, the signal transmission (via phosphatase or kinase activity on the C-terminal, anti-σ factor antagonist, STAS domain) in Rv1364c depends on the structure of the dimer or, more likely, on a dimer-monomer interconversion. The long linker between the C-terminal domain and the rest of the protein is important since it could allow considerable flexibility of the C-terminal domain. It is noticeable that in the rigid body modeling against the SAXS data it is the C-terminal STAS domain (cyan in Figures 5D and 5E) that fits least well into the determined ab initio envelope. This flexibilty is of functional relevance since the C-terminal domain is reported to interact with both the Rv1364c$_{169\text{-}399}$ (phosphatase) and Rv1364c$_{403\text{-}527}$ (kinase) domains (Parida et al., 2005). In this process, the C-terminal domain is dephosphorylated or phosphorylated, respectively (Greenstein et al., 2009). From the crystal structures, four different dimerization interfaces are possible (see also Supplemental Information). One is from the N-terminal PAS domain (Rv1364c$_{1\text{-}156}$), one from the phosphatase domain (Rv1364c$_{169\text{-}399}$), and two from the kinase domain (Rv1364c$_{402\text{-}527}$). The dimer in solution, as indicated by the ab initio envelope, suggests a head to tail dimer with 2-fold symmetry perpendicular to the longest axis of the dimer. This eliminates the PAS domain as a determinant of the dimer interface since this domain exhibits a head to head arrangement (see molecules A and B in Figure 1D). The different dimerization interfaces from the three remaining interfaces failed to produce dimers that fit the scattering data or the derived ab initio envelope of the full-length protein especially well. This leads us to suggest that the signal transduction might be dependent upon the monomer-dimer interconversion.

Palmitic and palmitoleic acids are the most common FAs found in *E. coli* (Mair and Ingram, 1962; Khuller et al., 1982) and so it is no surprise to find them bound to a FA-binding domain when it is heterologously expressed in *E. coli*. The fact that not all the PAS domain structures reported here have bound FA probably results from the nature of the (necessary) purification protocol. This is, however, the first reported structure of a PAS domain with bound FA. We have not been able to obtain any structural data on PAS domains with bound palmitoleic acid, despite its higher affinity. Nor have we investigated differences in activity of the full-length protein with different FAs bound. These desirable investigations must be left to others. Potential reasons as to why FAs might act as signaling molecules are interesting, but at this point in time purely speculative. In this context we note that the longer PAS construct does bind retinol but too weakly to be able to characterize the binding. We also note that temperature changes in bacteria alter the distribution of saturated versus unsaturated fatty acids (Teng et al., 1997), and we were intrigued that the PAS domain of Rv1364c binds palmitoleic acid in preference to palmitic acid. However *M. tuberculosis* exhibits optimum growth at around human body temperature and therefore it is unlikely that the PAS domain is acting as part of a temperature switch.

Finally the PAS domain of RsbP from *B. subtilis* has recently been crystallized (Makino et al., 2009) but no structural data are yet available. It will be very interesting to establish whether that PAS domain also binds FAs.

EXPERIMENTAL PROCEDURES

Cloning, Expression, and Purification

Rv1364c, Rv1364c$_{1\text{-}147}$, Rv1364c$_{1\text{-}156}$, and Rv1364c$_{169\text{-}539}$ were PCR amplified from *Mycobacterium tuberculosis* H37Rv genomic DNA using Phusion high-fidelity DNA polymerase (New England Biolabs). The primers were as follows:

Rv1364c-fwd ATTACCATGGCGGCCGAAATGGACTGGGACAAAACGG,
Rv1364c-rev AACCGGAAGCTTATTACTCCTGGGCGAAGATGTCC,
Rv1364c$_{n\text{-}147}$-rev CGTAGAAGCTTATTAGCGCTCGGACAGTTCCTC,
Rv1364c$_{n\text{-}156}$-rev GCCCGAAGCTTACTAATCGCGCACATTGCGATA,
Rv1364c$_{169\text{-}n}$-fwd AAATCCATGGTTTCGGTGCCCGTGGTTCCCGGC,
Rv1364c$_{n\text{-}539}$-rev CGAAGCTTATTACCGGCGAACCATCGTGTC.

The amplified PCR products were examined by agarose gel analysis and subsequently purified using a QIAGEN GEL extraction kit according to the kit's protocol. The purified PCR product was prepared for ligation by restriction endonuclease (NcoI and HindIII) digestion followed by further purification using the QIAGEN PCR purification kit according to the manufacturer's instructions. The digested PCR product was then cloned into a similarly digested pETM-11 (EMBL) expression vector. Cloning was verified through sequence analysis by MWG-Biotech. The PCR products were ligated with T4 DNA ligase into the pETM-11 expression vector with an N-terminal His$_6$-tag. The plasmid for Rv1364c$_{169\text{-}539}$ was transformed into Rosetta(DE3)pLysS cells and the others were transformed into BL21(DE3)pRPpLysS cells. Cells were induced with 1 mM IPTG at OD_{600} = 0.6 and were grown overnight at 16°C. The cells were harvested by centrifugation and lysed by sonication in buffer A (50 mM Tris-HCl [pH 8.0], 100 mM NaCl, 0.02% monothioglycerol for Rv1364c$_{1\text{-}147}$, 20 mM Tris-HCl [pH 8.0], 100 mM NaCl, 0.02% monothioglycerol for Rv1364c$_{1\text{-}156}$ and 50 mM HEPES [pH 7.4], 300 mM NaCl, 10% glycerol and 0.02% monothioglycerol for Rv1364c$_{169\text{-}539}$) plus 1 μg ml^{-1} DNaseI, 5 mM $MgCl_2$ and protease inhibitors. The lysate was spun down before being applied to a Ni-NTA column equilibrated in buffer A. The protein was eluted by applying the elution buffer in a linear 75 ml gradient of 10–250 mM of imidazole.

For expression of selenomethionine containing protein, the pETM-11 expression vector containing the Rv1364c$_{1\text{-}147}$ insert was transformed into the *E. coli* strain B834(DE3)pLysS. The transformed cells were plated on to LB plates containing kanamycin and chloramphenicol and incubated overnight at 37°C. A preculture of 1 × M9 minimal media was inoculated with a single colony and the appropriate antibiotics. All the amino acids (76 mg of each) with the exception of methionine were added to the preculture which was incubated at 37°C overnight. The following day 4 × 1 liter flasks of 1 × M9 minimal media were set up with the appropriate antibiotics. Each flask contained 760 mg of all the amino acids (excluding methionine) and 600 mg of seleno-L-methionine. 250 ml of the preculture was used to inoculate each flask. The cultures were then incubated at 37°C until an OD_{600} of 0.7 was reached. The cultures were then induced with 1 mM IPTG each and incubated at 16°C for 48 hr. Finally the cultures were harvested by centrifugation and the cell pellets were stored at −20°C. Purification was as for the native protein.

Crystallization

Crystallization was carried out at 19°C using the hanging drop vapor diffusion method. Crystals of Rv1364c$_{1\text{-}147}$ were obtained from 1 μl of protein solution at 10 mg ml^{-1} (in 20 mM Tris HCl [pH 8.0], 100 mM NaCl, 0.02% v/v monothioglycerol) and 1 μl of reservoir solution (1.4 M $(NH_4)_2SO_4$, 0.1 M Tris HCl [pH 8.0] and 0.1 M NaCl). Crystals of Rv1364c$_{1\text{-}156}$ were obtained from 1 μl of protein solution at 13 mg ml^{-1} (in 20 mM Tris HCl [pH 8.0], 100 mM NaCl, 0.02% v/v

Table 4. $Rv1364c_{1-147}$ and $Rv1364c_{1-156}$ Data Collection and Refinement Statistics

Data Collection[a]	$Rv1364c_{1-147}$ Selenomethionine Peak	$Rv1364c_{1-147}$ Selenomethionine Inflection Point	$Rv1364c_{1-147}$ Selenomethionine High-Energy Remote	$Rv1364c_{1-156}$
Beamline	X12	X12	BW7A	X13
Wavelength (Å)	0.978	0.977	0.972	0.808
Space group	$P6_222$	$P6_222$	$P6_222$	$C2$
Cell parameters (Å,°)	a = b = 60.1,	a = b = 59.9,	a = b = 60.1,	a = 209.1, b = 63.8,
	c = 172.0	c = 172.0	c = 171.9	c = 61.3, β = 90.5
Maximum resolution (Å)	2.7	2.6	2.3	1.62
Nr. of unique reflections	5 561	6 232	8 299	102 879
Completeness (%)	100.0 (100.0)	100.0 (100.0)	100.0 (100.0)	95.3 (98.6)
Multiplicity	50.1 (21.8)	40.2 (40.5)	21.2 (22.4)	5.0 (4.9)
$I/\sigma(I)$[b]	64.27 (8.89)	45.75 (4.97)	39 (4.69)	18.87 (2.78)
Rsym[c] (%)	10.7 (73.7)	10.6 (72.1)	7.6 (74.1)	8.7 (65.4)
Rp.i.m[d] (%)	1.7 (27.2)	1.9 (18.7)	1.7 (16.1)	4.3 (31.0)
Refinement				
Resolution (Å)			20.0–2.30	20.0–1.62
Rwork[e]/Rfree[f] (%)			24.5/29.5	18.1/21.2
Nr. of molecules in ASU			1	4
Nr. of residues			128	604
Nr. missing residues			19	20
Nr. of water molecules			22	657
Nr. of FA molecules			0	2
Nr. of glycerol molecules			0	11
Nr. of sulfate ions			0	6
Rmsd bonds (Å)			0.011	0.012
Rmsd angles (°)			1.3	1.4
PDB ID			3K3D	3K3C
Ramachandran plot[g]				
Most favored (%)			85.8	91.7
Additionally allowed (%)			14.2	7.9
Generously allowed (%)			0.0	0.4
Disallowed (%)			0.0	0.0

[a] Numbers given in brackets are from the last resolution shell.
[b] I is the integrated intensity and $\sigma(I)$ is the estimated standard deviation of that intensity.
[c] Rsym = $(\Sigma_{hkl}\Sigma_i|I_i(hkl)- < I(hkl) >|)/\Sigma_{hkl}\Sigma I_i(hkl)$, where $I_i(hkl)$ is the intensity of the ith measurement of reflection (hkl) and $< I(hkl) >$ is the average intensity.
[d] *Rp.i.m.* (Weiss, 2001) = $(\Sigma_{hkl}[1/N-1]^{1/2}\Sigma_i|I_i(hkl)- < I(hkl) >|)/\Sigma_{hkl}\Sigma I_i(hkl)$, where $I_i(hkl)$ is the intensity of the ith measurement of reflection (hkl), $< I(hkl) >$ is the average intensity and N is the number of measurements (or redundancy).
[e] Rwork = $(\Sigma_{hkl}|Fo-Fc|/\Sigma_{hkl}Fo$ where Fo and Fc are the observed and calculated structure factors.
[f] Rfree (Brunger, 1992) is calculated as for Rwork but from a randomly selected subset of the data (5%) which were excluded from the refinement.
[g] Ramachandran et al. (1963).

monothioglycerol) and 1 μl of reservoir solution (1.4 M $[NH_4]_2SO_4$, 0.1 M Tris HCl [pH 8.0] and 0.1 M NaCl). Crystals of $Rv1364c_{169-539}$ were obtained from 1 μl of protein solution at 25 mg ml^{-1} (in 50 mM HEPES [pH 7.4], 300 mM NaCl, 10% v/v glycerol, 0.02% v/v monothioglycerol) and 1 μl of reservoir solution (1.2 M $[NH_4]_2SO_4$, 50 mM ADA [pH 6.5]). They diffracted poorly but an additive screen initially identified calcium acetate, subsequently replaced by $MnCl_2$, as a requirement for good diffraction. Crystals of $Rv1364c_{1-147}$ and $Rv1364c_{1-156}$ were cryoprotected with 23% glycerol. Crystals of $Rv1364c_{169-539}$ were cryoprotected with 10 mM $MnCl_2$, 10 mM Tris HCl (pH 7.5), 20% glycerol, and 8% DMSO.

Data Collection and Structure Solution

X-ray data were collected variously on the X12, X13, and BW7A beamlines of the EMBL Hamburg Outstation at DESY using MAR225 or MAR165 CCD detectors. Data collection and refinement details are given in Tables 4 and 5. Reflections were indexed and integrated using DENZO (Minor et al., 2000) and scaled using SCALEPACK (Otwinowski et al., 2003). Intensities were converted to structure amplitudes using TRUNCATE of the CCP4 package (CCP4, 1994; Winn et al., 2002).

The crystal structures of the two PAS domain constructs ($Rv1364c_{1-147}$ and $Rv1364c_{1-156}$) were determined using initial phases from a two-wavelength anomalous diffraction experiment on selenomethionine (SeMet) substituted protein crystals of the shorter construct. The initial model of the shorter construct was manually built at a resolution of 2.6 Å and then refined against 2.3 Å data collected from a second SeMet crystal. Both selenium atoms were found using the program SHELXD (Schneider and Sheldrick, 2002) and the correct hand for the substructure determined using SHELXE (Sheldrick, 2002). The selenium atoms were refined and initial phases calculated using

Table 5. $Rv1364c_{169-539}$ Data Collection and Refinement Statistics

Data Collection[a]	Peak	Inflection Point	Remote	Native (Ca)	Native (Mn) High Energy
Beamline	X12	X12	X12	X12	X12
Wavelength (Å)	1.890	1.892	1.771	0.979	1.000
Space group	$P4_32_12$	$P4_32_12$	$P4_32_12$	$P4_32_12$	$P4_32_12$
Cell parameters (Å)	a = b = 101.0,	a = b = 101.2,	a = b = 101.4,	a = b = 99.9,	a = b = 100.1,
	c = 170.2	c = 170.7	c = 171.1	c = 169.6	c = 169.7
Maximum resolution (Å)	2.95	3.00	3.06	2.80	2.60
Nr. of unique reflections	19 200	18 555	17 496	21 815	27 381
Completeness (%)	100.0 (100.0)	100.0 (100.0)	100.0 (100.0)	100.0 (100.0)	99.3 (98.0)
Multiplicity	28.3 (28.3)	28.3 (28.4)	28.5 (28.8)	29.1 (29.6)	15.2 (14.1)
$I/\sigma(I)$ [b]	29.8 (3.13)	26.9 (2.3)	27.5 (2.01)	23.5 (3.2)	25.5 (2.7)
Rsym[c] (%)	13.3 (57.5)	13.6 (60.2)	12.2 (59.2)	17.1 (72.0)	11.8 (72.7)
Rp.i.m[d] (%)	2.7 (23.1)	2.9 (31.8)	2.9 (37.4)	3.6 (26.6)	3.1 (30.4)
Refinement					
Resolution (Å)					19.63–2.60
Rwork[e]/Rfree[f] (%)					20.8/26.7
Nr. of molecules in ASU					2
Nr. of residues					704
Nr. missing residues					94
Nr. of water molecules					115
Nr. of Mn(II) ions					4
Nr. of glycerol molecules					1
Nr. of sulfate ions					1
Rmsd bonds (Å)					0.012
Rmsd angles (°)					1.4
PDB ID					3KE6
Ramachandran plot[g]					
Most favored (%)					93.5
Additionally allowed (%)					6.2
Generously allowed (%)					0.3
Disallowed (%)					0.0

[a] Numbers given in brackets are from the last resolution shell.
[b] I is the integrated intensity and $\sigma(I)$ is the estimated standard deviation of that intensity.
[c] Rsym = $(\Sigma_{hkl}\Sigma_i|I_i(hkl)- < I(hkl) >I)/\Sigma_{hkl}\Sigma I_i(hkl)$, where $I_i(hkl)$ is the intensity of the ith measurement of reflection (hkl) and $< I(hkl) >$ is the average intensity.
[d] Rp.i.m. (Weiss, 2001) = $(\Sigma_{hkl}[1/N-1]^{1/2}\Sigma_i|I_i(hkl)- < I(hkl) >I)/\Sigma_{hkl}\Sigma I_i(hkl)$, where $I_i(hkl)$ is the intensity of the ith measurement of reflection (hkl), $< I(hkl) >$ is the average intensity and N is the number of measurements (or redundancy).
[e] Rwork = $(\Sigma_{hkl}|Fo-Fc|/\Sigma_{hkl}Fo$ where Fo and Fc are the observed and calculated structure factors.
[f] Rfree (Brunger, 1992) is calculated as for Rwork but from a randomly selected subset of the data (5%) which were excluded from the refinement.
[g] Ramachandran et al. (1963).

MLPHARE (CCP4, 1994). These phases were improved using DM (Cowtan, 1994) and a partial model built automatically by ARP/wARP (Perrakis et al., 1999). Manual model building using COOT (Emsley and Cowtan, 2004) and refinement using CNS and REFMAC5 (Murshudov et al., 1997) were used to extend and improve the model. The single molecule in the ASU (Figure 1A) shows good electron density for all residues except −1–4, 96–102, and 139–147. Coordinates and structure factors for the final model of $Rv1364c_{1-147}$ have been deposited in the PDB (Berman et al., 2002) as entry 3K3D.

The $Rv1364c_{1-147}$ structure was then used as a search model for the $Rv1364c_{1-156}$, construct using the molecular replacement program MOLREP (Vagin and Teplyakov, 2000). Automated model building using ARP/wARP (Perrakis et al., 1999) followed by manual model completion using COOT (Emsley and Cowtan, 2004) and model refinement using REFMAC5 (Murshudov et al., 1997; Winn et al., 2001)gave (Figure 1D) an almost complete build of all four molecules in the ASU. The final model misses 6 residues at the N terminus of all molecules and two residues at the C terminus of molecules C and D. Coordinates and structure factors have been deposited in the PDB as entry 3K3C.

The structure of $Rv1364c_{169-539}$ was determined with experimental phases obtained from a three wavelength anomalous diffraction experiment using a single crystal soaked overnight in the $MnCl_2$ containing cryobuffer. The 16 manganese sites in the ASU gave an initial experimental electron density map at 3.05 Å resolution. A 2.6 Å data set collected from another crystal (soaked for 5 min in the cryobuffer and which, therefore, only contained the four Mn^{2+} ions bound in the phosphatase active site) at a wavelength of 1.0 Å was then used for model building and refinement.

The initial electron density and a partial model were obtained using the 3W-MAD protocol of Auto-Rickshaw (Panjikar et al., 2005). FA values were calculated using the program SHELXC (Sheldrick et al., 2001). Sixteen heavy atoms were found using the program SHELXD (Schneider and Sheldrick, 2002). The correct hand for the substructure was determined using the programs ABS and SHELXE (Sheldrick, 2002). The occupancy of all

substructure atoms was refined and initial phases were calculated using the program SHARP (Bricogne et al., 2003). The initial phases were improved using density modification and phase extension to 3.0 Å resolution using the program DM (Cowtan, 1994). HELICAP (Morris et al., 2004) was employed for initial model building and built 178 Cαs in 18 separate chains. Manual model building was carried out using the non-NCS averaged DM maps. The PDB entries 1TXO and 1L0O were used as templates to build a hybrid model to fit to the electron density prior to a phased molecular replacement with MOLREP (Vagin and Teplyakov, 1997).

The heavy atom sites were redetermined by calculating an anomalous difference Fourier map. With the calculated heavy atoms sites as input, the program RESOLVE (Terwilliger, 2000) was used to accurately determine the NCS operator. After statistical density modification and NCS averaging RESOLVE built 442 residues without side chains in each NCS copy. The resulting model was manually rebuilt with the program COOT (Emsley and Cowtan, 2004) using the PDB entry 1TXO as a guide for the phosphatase domain. Once a complete model had been built in the 3.05 Å maps a mask of the protein was generated using the program MAMA (Kleywegt and Jones, 1999). Since both the calcium-derived data (2.8 Å) and high-resolution manganese-derived (2.6 Å) data appeared to be slightly nonisomorphous to the 3W-MAD data, their NCS operators were determined using a single monomer from the 3.05 Å model using MOLREP. The mask, the NCS operators, the manganese-derived data (2.6 Å), calcium-derived data (2.8 Å), and the MAD data (3.05 Å) with the initial phases were used as input for multiple crystal density modification with NCS averaging, solvent flattening and histogram mapping with the program DMMULTI (Cowtan et al., 2001). The program MAID (Levitt, 2001) was used to build the model from scratch in the newly created DM 2.8 Å maps. This model (612 residues) was then manually rebuilt using the program COOT and docked to the known sequence. Subsequent model building was carried out with iterative rounds of refinement using the simulated annealing protocol of the CNS package. Once the R factor was below 30% refinement was carried out using the program REFMAC5. The resulting model was then used to refine the 2.6 Å data with COOT and REFMAC5. Refinement cycles consisted of bulk solvent correction, anisotropic scaling, and a multiple rigid body TLS refinement. The overall geometric quality of the model was assessed using the program PROCHECK (Laskowski et al., 1993). Coordinates and structure factors have been deposited in the PDB as entry 3KE6.

The additional manganese binding sites for the crystals soaked overnight in $MnCl_2$ occur principally between molecules and have lower occupancies.

Fatty Acid Binding

The fatty acids oleic acid, palmitic acid, palmitoleic acid, arachidonic acid, and retinol were dissolved in ethanol to a concentration of either 1.0 or 0.1 mM. Steady-state fluorescence was measured with a Fluorimax spectrophotometer at room temperature. Prior to the experiment $Rv1364c_{1\text{-}156}$was treated with the LIPIDEX-1000 matrix in order to extract any copurified fatty acids. The $Rv1364c_{1\text{-}156}$ protein solution at a concentration of 1 mg ml^{-1} was incubated with 1 ml of the LIPIDEX-1000 matrix resuspended in 10 mM Tris·HCl (pH 8.0). The mixture was incubated at 37°C for 1 hr. Following incubation, the mixture was centrifuged and the solute was decanted and reapplied to a fresh solution of the resuspended matrix. The incubation was then repeated. The whole process was repeated six times.

Ligand binding experiments were performed with 1.2 μM of $Rv1364c_{1\text{-}156}$ in a sample volume of 800 μl. Binding affinities were studied by changes in the intrinsic tryptophan emission of the protein using an excitation wavelength (λ*ex*) of 295 nm and an emission wavelength (λ*em*) of 345 nm. All ligands were monitored by measuring changes in the emission intensity at λ*em* = 345 nm. The titrations were performed in 10 mM Tris HCl (pH 7.5). The concentration of the organic solvent in the final reaction did not exceed 2.5%. Because retinol absorbs at both λ*ex* = 295 nm and λ*em* = 345 nm, its emission spectra were corrected for an inner filter effect. In order to minimize inner filter and self- absorption effects, absorption of the samples at λ*ex* was always less than 0.05. All emission spectra were corrected for progressive dilution. The apparent dissociation constant (K_D) and maximal fluorescence change upon saturation of the $Rv1364c_{1\text{-}156}$ binding site (Δ*Fmax*) were calculated from the experimental data, which was analyzed using the GraphPad Prism program. The data were analyzed by a nonlinear regression and fitted to a one-site binding hyperbola, $\Delta Fobs = (\Delta Fmax[L])/(K_D+[L])$, where Δ*Fobs* is the observed change in the fluorescence and [*L*] is the ligand concentration.

Phosphatase Activity Assay

The activity of the full-length protein Rv1364c and the smaller phosphatase containing construct $Rv1364c_{169\text{-}539}$ were assayed with the nonspecific substrate *p*-nitrophenol phosphate. The assays were carried out at pH 7.5 with 25 mM Tris HCl, 50 mM NaCl, 0.02% monothioglycerol and 5 mM $MnCl_2$ or 5 mM $MgCl_2$. The formation of *p*-nitrophenol was observed at 410 nm.

Small-Angle X-ray Scattering Measurements

Following size exclusion chromatography, where Rv1364c elutes primarily as a dimer with a small monomeric fraction, both fractions of the full-length Rv1364c were analyzed in solution by SAXS. All data were collected at the X33 beamline using the MAR345 image plate detector (Roessle et al., 2007). The scattering patterns were measured with a 3 min exposure time for a monomeric sample with a stock concentration of 4.1 mg/ml (and its 2- and 4-fold dilutions) and a dimeric sample with a concentration of 6.7 mg/ml (and its 2- and 4-fold dilutions). No concentration effect was observed. No radiation damage was detected, as verified by comparing duplicate scattering patterns from 2 min exposures. Using a sample-detector distance of 2.7 m, the momentum transfer range $0.009 < s < 0.5$ $Å^{-1}$ was covered (where $s = 4\pi\sin(\theta)/\lambda$, 2θ is the scattering angle, and λ = 1.5 Å the X-ray wavelength). The data was processed using the PRIMUS (Konarev et al., 2003) program package and standard procedures. The forward scattering (*I*(0)) and the radius of gyration (R_g) were evaluated using the Guinier approximation assuming that at very small angles ($s < 1.3/R_g$) the intensity is represented as $I(s) = I(0)\exp(-(sR_g)^2/3)$.

The program GNOM (Svergun, 1992) was used to calculate D*max* and the interatomic distance distribution function *p*(*r*). The molecular mass (MM_{exp}) for each oligomeric form was evaluated by a comparison of the forward scatter for each sample with that from the reference protein solution of bovine serum albumin (MM = 66 kDa). The particle shape of each oligomer was reconstructed ab initio using the programs DAMMIN (Svergun, 1999) and GASBOR (Svergun et al., 2001). The scattering patterns of the atomic crystal structures for $Rv1364c_{1\text{-}156}$ and $Rv1364c_{169\text{-}539}$ were calculated using the program CRYSOL. An atomic model of the C-terminal domain (residues 561–653) was generated using MODELER (Sali and Blundell, 1993) based upon two crystal structures of the anti-σ factor antagonists SpoIIAA (PDB ID:1TH8 [Masuda et al., 2004]) from *B. subtilis* and TM1442 (PDB ID:1VC1 (Lee et al., 2004) from *T. maritima*. The program BUNCH (Petoukhov and Svergun, 2005) was employed to model the position and orientation of the two crystal structures and the C-terminal domain model against the monomeric and dimeric SAXS data. The two linker regions: linker 1 (11 residues) and linker 2 (28 residues) were also modeled as Cα atoms by BUNCH connecting $Rv1364c_{1\text{-}156}$ to $Rv1364c_{169\text{-}539}$ and $Rv1364c_{169\text{-}539}$ to the C-terminal domain, respectively. The domain interface between the anti-σ factor (SpoIIAB) and the anti-σ factor antagonist (SpoIIAA) (PDB ID: 1TH8 [Masuda et al., 2004]) was used as a template for the initial manually generated input model used by BUNCH. For the ab initio analyses and modeling, multiple runs were performed to verify the stability of the solution.

ACCESSION NUMBERS

Coordinates and structure factors have been deposited in the Protein Data Bank under ID codes 3K3C, 3K3D, and 3KE6.

SUPPLEMENTAL INFORMATION

Supplemental Information includes five figures and one movie and can be found with this article online at doi:10.1016/j.str.2010.11.010.

ACKNOWLEDGMENTS

We thank the Bundesministerium für Bildung, und Forschung (German Science Ministry) funded X-MTBconsortium (http://xmtb.org/start.html) for infrastructural support.

Received: February 22, 2010
Revised: November 15, 2010
Accepted: November 16, 2010
Published: January 11, 2011

REFERENCES

Almo, S.C., Bonanno, J.B., Sauder, J.M., Emtage, S., Dilorenzo, T.P., Malashkevich, V., Wasserman, S.R., Swaminathan, S., Eswaramoorthy, S., Agarwal, R., et al. (2007). Structural genomics of protein phosphatases. J. Struct. Funct. Genomics *8*, 121–140.

Alper, S., Dufour, A., Garsin, D.A., Duncan, L., and Losick, R. (1996). Role of adenosine nucleotides in the regulation of a stress-response transcription factor in Bacillus subtilis. J. Mol. Biol. *260*, 165–177.

Babson, A.L., and Phillips, G.E. (1966). An improved acid phosphatase procedure. Clin. Chim. Acta Int. J. Clin. Chem. *13*, 264–265.

Ban, C., Junop, M., and Yang, W. (1999). Transformation of MutL by ATP binding and hydrolysis: a switch in DNA mismatch repair. Cell *97*, 85–97.

Barford, D., Das, A.K., and Egloff, M.P. (1998). The structure and mechanism of protein phosphatases: insights into catalysis and regulation. Annu. Rev. Biophys. Biomol. Struct. *27*, 133–164.

Benson, A.K., and Haldenwang, W.G. (1992). Characterization of a regulatory network that controls sigma B expression in Bacillus subtilis. J. Bacteriol. *174*, 749–757.

Benson, A.K., and Haldenwang, W.G. (1993). Regulation of sigma B levels and activity in Bacillus subtilis. J. Bacteriol. *175*, 2347–2356.

Bergerat, A., de Massy, B., Gadelle, D., Varoutas, P.C., Nicolas, A., and Forterre, P. (1997). An atypical topoisomerase II from Archaea with implications for meiotic recombination. Nature *386*, 414–417.

Berman, H.M., Battistuz, T., Bhat, T.N., Bluhm, W.F., Bourne, P.E., Burkhardt, K., Feng, Z., Gilliland, G.L., Iype, L., Jain, S., et al. (2002). The Protein Data Bank. Acta Crystallogr. D Biol. Crystallogr. *58*, 899–907.

Betts, J.C., Lukey, P.T., Robb, L.C., McAdam, R.A., and Duncan, K. (2002). Evaluation of a nutrient starvation model of Mycobacterium tuberculosis persistence by gene and protein expression profiling. Mol. Microbiol. *43*, 717–731.

Bilwes, A.M., Quezada, C.M., Croal, L.R., Crane, B.R., and Simon, M.I. (2001). Nucleotide binding by the histidine kinase CheA. Nat. Struct. Biol. *8*, 353–360.

Bork, P., Brown, N.P., Hegyi, H., and Schultz, J. (1996). The protein phosphatase 2C (PP2C) superfamily: detection of bacterial homologues. Protein Sci. *5*, 1421–1425.

Boylan, S.A., Rutherford, A., Thomas, S.M., and Price, C.W. (1992). Activation of Bacillus subtilis transcription factor sigma B by a regulatory pathway responsive to stationary-phase signals. J. Bacteriol. *174*, 3695–3706.

Bricogne, G., Vonrhein, C., Flensburg, C., Schiltz, M., and Paciorek, W. (2003). Generation, representation and flow of phase information in structure determination: recent developments in and around SHARP 2.0. Acta Crystallogr. D Biol. Crystallogr. *59*, 2023–2030.

Brunger, A.T. (1992). Free R value: a novel statistical quantity for assessing the accuracy of crystal structures. Nature *355*, 472–475.

Campbell, E.A., Masuda, S., Sun, J.L., Muzzin, O., Olson, C.A., Wang, S., and Darst, S.A. (2002). Crystal structure of the Bacillus stearothermophilus anti-sigma factor SpoIIAB with the sporulation sigma factor sigmaF. Cell *108*, 795–807.

CCP4 Collaborative Computational Project, Number 4. (1994). The CCP4 suite: programs for protein crystallography. Acta Crystallogr. D Biol. Crystallogr. *50*, 760–763.

Coe, N.R., and Bernlohr, D.A. (1998). Physiological properties and functions of intracellular fatty acid-binding proteins. Biochim. Biophys. Acta *1391*, 287–306.

Cohen, P. (1994). The discovery of protein phosphatases: from chaos and confusion to an understanding of their role in cell regulation and human disease. Bioessays *16*, 583–588.

Cowtan, K. (1994) Joint CCP4 and ESF–EACBM Newsletter on protein crystallography. *31*, 34–38.

Cowtan, K.D., Zhang, K.Y.J., and Main, P. (2001). DM/DMMULTI software for phase improvement by density modification. In International Tables for Crystallography, Volume F. Crystallography of Biological Macromolecules. Rossmann, M.G., Arnold, E., eds. (Dordrecht, Netherlands: Kluwer Academic Publishers), pp. 705–710.

Das, A.K., Helps, N.R., Cohen, P.T., and Barford, D. (1996). Crystal structure of the protein serine/threonine phosphatase 2C at 2.0 A resolution. EMBO J. *15*, 6798–6809.

DeMaio, J., Zhang, Y., Ko, C., Young, D.B., and Bishai, W.R. (1996). A stationary-phase stress-response sigma factor from Mycobacterium tuberculosis. Proc. Natl. Acad. Sci. USA *93*, 2790–2794.

DeMaio, J., Zhang, Y., Ko, C., and Bishai, W.R. (1997). Mycobacterium tuberculosis sigF is part of a gene cluster with similarities to the Bacillus subtilis sigF and sigB operons. Tuber. Lung Dis. *78*, 3–12.

Duncan, L., and Losick, R. (1993). SpoIIAB is an anti-sigma factor that binds to and inhibits transcription by regulatory protein sigma F from Bacillus subtilis. Proc. Natl. Acad. Sci. USA *90*, 2325–2329.

Dutta, R., and Inouye, M. (2000). GHKL, an emergent ATPase/kinase superfamily. Trends Biochem. Sci. *25*, 24–28.

Emsley, P., and Cowtan, K. (2004). Coot: model-building tools for molecular graphics. Acta Crystallogr. D Biol. Crystallogr. *60*, 2126–2132.

Genick, U.K., Soltis, S.M., Kuhn, P., Canestrelli, I.L., and Getzoff, E.D. (1998). Structure at 0.85 A resolution of an early protein photocycle intermediate. Nature *392*, 206–209.

Gong, W., Hao, B., Mansy, S.S., Gonzalez, G., Gilles-Gonzalez, M.A., and Chan, M.K. (1998). Structure of a biological oxygen sensor: a new mechanism for heme-driven signal transduction. Proc. Natl. Acad. Sci. USA *95*, 15177–15182.

Greenstein, A.E., Hammel, M., Cavazos, A., and Alber, T. (2009). Interdomain communication in the Mycobacterium tuberculosis environmental phosphatase Rv1364c. J. Biol. Chem. *284*, 29828–29835.

Gilles-Gonzalez, M.A., and Gonzalez, G. (2004). Signal transduction by heme-containing PAS-domain proteins. J. Appl. Physiol. *96*, 774–783.

Hardwick, S.W., Pané-Farré, J., Delumeau, O., Marles-Wright, J., Murray, J.W., Hecker, M., and Lewis, R.J. (2007). Structural and functional charcterization of partner switching regulating the environmental stress response in Bacillus subtilis. J. Biol. Chem. *282*, 11562–11572.

Hefti, M.H., Francoijs, K.J., de Vries, S.C., Dixon, R., and Vervoort, J. (2004). The PAS fold. A redefinition of the PAS domain based upon structural prediction. Eur. J. Biochem. *271*, 1198–1208.

Jackson, M.D., Fjeld, C.C., and Denu, J.M. (2003). Probing the function of conserved residues in the serine/threonine phosphatase PP2Calpha. Biochemistry *42*, 8513–8521.

Jones, T.A., Bergfors, T., Sedzik, J., and Unge, T. (1988). The three-dimensional structure of P2 myelin protein. EMBO J. *7*, 1597–1604.

Kaufmann, S.H., and McMichael, A.J. (2005). Annulling a dangerous liaison: vaccination strategies against AIDS and tuberculosis. Nat. Med. *11*, S33–S44.

Kennelly, P.J., and Potts, M. (1996). Fancy meeting you here! A fresh look at "prokaryotic" protein phosphorylation. J. Bacteriol. *178*, 4759–4764.

Key, J., Hefti, M., Purcell, E.B., and Moffat, K. (2007). Structure of the redox sensor domain of Azotobacter vinelandii NifL at atomic resolution: signaling, dimerization, and mechanism. Biochemistry *46*, 3614–3623.

Khuller, G.K., Taneja, R., Kaur, S., and Verma, J.N. (1982). Lipid composition and virulence of Mycobacterium tuberculosis H37Rv. Aust. J. Exp. Biol. Med. Sci. *60*, 541–547.

Kleywegt, G.J., and Jones, T.A. (1999). Software for handling macromolecular envelopes. Acta Crystallogr. D Biol. Crystallogr. *55*, 941–944.

Konarev, P.V., Volkov, V.V., Sokolova, A.V., Koch, M.H.J., and Svergun, D.I. (2003). PRIMUS: a Windows PC-based system for small-angle scattering data analysis. J. Appl. Crystallogr. *36*, 1277–1282.

Krissinel, E., and Henrick, K. (2004). Secondary-structure matching (SSM), a new tool for fast protein structure alignment in three dimensions. Acta Crystallogr. D Biol. Crystallogr. *60*, 2256–2268.

Krissinel, E., and Henrick, K. (2007). Inference of macromolecular assemblies from the crystalline state. J. Mol. Biol. *372*, 774–797.

Krissinel, E., and Henrick, K. (2004). Secondary-structure matching (SSM), a new tool for fast protein structure alignment in three dimensions. Acta Crystallogr. D Biol. Crystallogr. *60*, 2256–2268.

Laskowski, R.A., MacArthur, M.W., Moss, D.S., and Thornton, J.M. (1993). PROCHECK: a program to check the stereochemical quality of protein structures. J. Appl. Crystallogr. *26*, 283–291.

Lee, J.Y., Ahn, H.J., Ha, K.S., and Suh, S.W. (2004). Crystal structure of the TM1442 protein from Thermotoga maritima, a homolog of the Bacillus subtilis general stress response anti-anti-sigma factor RsbV. Proteins *56*, 176–179.

Letunic, I., Doerks, T., and Bork, P. (2009). SMART 6: recent updates and new developments. Nucleic Acids Res. *37*, D229–D232.

Levitt, D.G. (2001). A new software routine that automates the fitting of protein X-ray crystallographic electron-density maps. Acta Crystallogr. D Biol. Crystallogr. *57*, 1013–1019.

Li, M.S., Waddell, S.J., Monahan, I.M., Mangan, J.A., Martin, S.L., Everett, M.J., and Butcher, P.D. (2004). Increased transcription of a potential sigma factor regulatory gene Rv1364c in Mycobacterium bovis BCG while residing in macrophages indicates use of alternative promoters. FEMS Microbiol. Lett. *233*, 333–339.

Mair, A.G., and Ingram, J.L. (1962). Effect of temperature on the composition of fatty acids in Escherichia coli. J. Bacteriol. *84*, 1260–1267.

Makino, M., Kondo, S., Kaneko, T., Baba, S., Hirata, K., and Kumasaka, T. (2009). Expression, crystallization and preliminary crystallographic analysis of the PAS domain of RsbP, a stress-response phosphatase from Bacillus subtilis. Acta Crystallogr. Sect. F Struct. Biol. Cryst. Commun. *65*, 559–561.

Malik, S.S., Luthra, A., and Ramachandran, R. (2009). Interactions of the M. tuberculosis UsfX with the cognate sigma factor SigF and the anti-anti sigma factor RsfA. Biochim. Biophys. Acta *1794*, 541–553.

Masuda, S., Murakami, K.S., Wang, S., Anders Olson, C., Donigian, J., Leon, F., Darst, S.A., and Campbell, E.A. (2004). Crystal structures of the ADP and ATP bound forms of the Bacillus anti-sigma factor SpoIIAB in complex with the anti-anti-sigma SpoIIAA. J. Mol. Biol. *340*, 941–956.

Min, K.T., Hilditch, C.M., Diederich, B., Errington, J., and Yudkin, M.D. (1993). Sigma F, the first compartment-specific transcription factor of B. subtilis, is regulated by an anti-sigma factor that is also a protein kinase. Cell *74*, 735–742.

Minor, W., Tomchick, D., and Otwinowski, Z. (2000). Strategies for macromolecular synchrotron crystallography. Structure *8*, R105–R110.

Miyatake, H., Mukai, M., Park, S.Y., Adachi, S., Tamura, K., Nakamura, H., Nakamura, K., Tsuchiya, T., Iizuka, T., and Shiro, Y. (2000). Sensory mechanism of oxygen sensor FixL from Rhizobium meliloti: crystallographic, mutagenesis and resonance Raman spectroscopic studies. J. Mol. Biol. *301*, 415–431.

Morris, R.J., Zwart, P.H., Cohen, S., Fernandez, F.J., Kakaris, M., Kirillova, O., Vonrhein, C., Perrakis, A., and Lamzin, V.S. (2004). Breaking good resolutions with ARP/wARP. J. Synchrotron. Radiat. *11*, 56–59.

Murshudov, G.N., Vagin, A.A., and Dodson, E.J. (1997). Refinement of macromolecular structures by the maximum-likelihood method. Acta Crystallogr. D Biol. Crystallogr. *53*, 240–255.

Otwinowski, Z., Borek, D., Majewski, W., and Minor, W. (2003). Multiparametric scaling of diffraction intensities. Acta Crystallogr. A *59*, 228–234.

Panjikar, S., Parthasarathy, V., Lamzin, V.S., Weiss, M.S., and Tucker, P.A. (2005). Auto-Rickshaw: an automated crystal structure determination platform as an efficient tool for the validation of an X-ray diffraction experiment. Acta Crystallogr. D Biol. Crystallogr. *61*, 449–457.

Parida, B.K., Douglas, T., Nino, C., and Dhandayuthapani, S. (2005). Interactions of anti-sigma factor antagonists of Mycobacterium tuberculosis in the yeast two-hybrid system. Tuberculosis (Edinb.) *85*, 347–355.

Pané-Farré, J., Lewis, R.J., and Stülke, J. (2005). The RsbRST stress module in bacteria: a signalling system that may interact with different output modules. J. Mol. Microbiol. *9*, 65–76.

Park, H., Suquet, C., Satterlee, J.D., and Kang, C. (2004). Insights into signal transduction involving PAS domain oxygen-sensing heme proteins from the X-ray crystal structure of Escherichia coli Dos heme domain (Ec DosH). Biochemistry *43*, 2738–2746.

Perrakis, A., Morris, R., and Lamzin, V.S. (1999). Automated protein model building combined with iterative structure refinement. Nat. Struct. Biol. *6*, 458–463.

Petoukhov, M.V., and Svergun, D.I. (2005). Global rigid body modeling of macromolecular complexes against small-angle scattering data. Biophys. J. *89*, 1237–1250.

Prodromou, C., Roe, S.M., O'Brien, R., Ladbury, J.E., Piper, P.W., and Pearl, L.H. (1997). Identification and structural characterization of the ATP/ADP-binding site in the Hsp90 molecular chaperone. Cell *90*, 65–75.

Pullen, K.E., Ng, H.L., Sung, P.Y., Good, M.C., Smith, S.M., and Alber, T. (2004). An alternate conformation and a third metal in PstP/Ppp, the M. tuberculosis PP2C-Family Ser/Thr protein phosphatase. Structure *12*, 1947–1954.

Ramachandran, G.N., Ramakrishnan, C., and Sasisekharan, V. (1963). Stereochemistry of polypeptide chain configurations. J. Mol. Biol. *7*, 95–99.

Rantanen, M.K., Lehtio, L., Rajagopal, L., Rubens, C.E., and Goldman, A. (2007). Structure of Streptococcus agalactiae serine/threonine phosphatase. The subdomain conformation is coupled to the binding of a third metal ion. FEBS J. *274*, 3128–3137.

Roessle, M.W., Klaering, R., Ristau, U., Robrahn, B., Jahn, D., Gehrmann, T., Konarev, P., Round, A., Fiedler, S., Hermes, C., and Svergun, D.I. (2007). Upgrade of the small-angle X-ray scattering beamline X33 at the European Molecular Biology Laboratory, Hamburg. J. Appl. Crystallogr. *40*, s190–s194.

Sacchettini, J.C., Gordon, J.I., and Banaszak, L.J. (1989). Refined apoprotein structure of rat intestinal fatty acid binding protein produced in Escherichia coli. Proc. Natl. Acad. Sci. USA *86*, 7736–7740.

Sachdeva, P., Narayan, A., Misra, R., Brahmachari, V., and Singh, Y. (2008). Loss of kinase activity in Mycobacterium tuberculosis multidomain protein Rv1364c. FEBS J. *275*, 6295–6308.

Sali, A., and Blundell, T.L. (1993). Comparative protein modelling by satisfaction of spatial restraints. J. Mol. Biol. *234*, 779–815.

Schneider, T.R., and Sheldrick, G.M. (2002). Substructure solution with SHELXD. Acta Crystallogr. D Biol. Crystallogr. *58*, 1772–1779.

Schultz, J., Milpetz, F., Bork, P., and Ponting, C.P. (1998). SMART, a simple modular architecture research tool: identification of signaling domains. Proc. Natl. Acad. Sci. USA *95*, 5857–5864.

Sheldrick, G.M. (2002). Macromolecular phasing with SHELXE. Z. Kristallogr. *217*, 644–650.

Sheldrick, G.M., Hauptman, H.A., Weeks, C.M., Miller, R., and Uson, I. (2001). Ab initio phasing. In International Tables for Crystallography, *Volume F*, E. Arnold, ed. (Dordrecht: Kluwer Academic Publishers), pp. 333–351.

Shi, X., Chen, M., Huvos, P.E., and Hardwicke, P.M. (1998). Amino acid sequence of a Ca(2+)-transporting ATPase from the sarcoplasmic reticulum of the cross-striated part of the adductor muscle of the deep sea scallop: comparison to serca enzymes of other animals. Comp. Biochem. Physiol. B Biochem. Mol. Biol. *120*, 359–374.

Svergun, D.I. (1992). Determination of the regularization parameter in indirect transform methods using perceptual criteria. J. Appl. Crystallogr. *25*, 495–503.

Svergun, D.I. (1999). Restoring low resolution structure of biological macromolecules from solution scattering using simulated annealing. Biophys. J. *76*, 2879–2886.

Svergun, D.I., Petoukhov, M.V., and Koch, M.H. (2001). Determination of domain structure of proteins from X-ray solution scattering. Biophys. J. *80*, 2946–2953.

Taylor, B.L., and Zhulin, I.B. (1999). PAS domains: internal sensors of oxygen, redox potential, and light. Microbiol. Mol. Biol. Rev. *63*, 479–506.

Taylor, S.S., and Radzio-Andzelm, E. (1994). Three protein kinase structures define a common motif. Structure *2*, 345–355.

Teng, L.J., Liaw, S.J., Hsueh, P.R., Fan, J.H., Luh, K.T., and Ha, S.W. (1997). Constitutive fatty acid and enzyme profiles of Mycobacterium species. J. Formos. Med. Assoc. *96*, 336–345.

Terwilliger, T.C. (2000). Maximum-likelihood density modification. Acta Crystallogr. D Biol. Crystallogr. *56*, 965–972.

Vagin, A., and Teplyakov, A. (1997). MOLREP: an automated program for molecular replacement. J. Appl. Crystallogr. *30*, 1022–1025.

Vagin, A., and Teplyakov, A. (2000). An approach to multi-copy search in molecular replacement. Acta Crystallogr. D Biol. Crystallogr. *56*, 1622–1624.

Vijay, K., Brody, M.S., Fredlund, E., and Price, C.W. (2000). A PP2C phosphatase containing a PAS domain is required to convey signals of energy stress to the sigmaB transcription factor of Bacillus subtilis. Mol. Microbiol. *35*, 180–188.

Voelker, U., Voelker, A., and Haldenwang, W.G. (1996). Reactivation of the Bacillus subtilis anti-sigma B antagonist, RsbV, by stress- or starvation-induced phosphatase activities. J. Bacteriol. *178*, 5456–5463.

Vreede, J., van der Horst, M.A., Hellingwerf, K.J., Crielaard, W., and van Aalten, D.M. (2003). PAS domains. Common structure and common flexibility. J. Biol. Chem. *278*, 18434–18439.

Wehenkel, A., Bellinzoni, M., Schaeffer, F., Villarino, A., and Alzari, P.M. (2007). Structural and binding studies of the three-metal center in two mycobacterial PPM Ser/Thr protein phosphatases. J. Mol. Biol. *374*, 890–898.

Weiss, M.S. (2001). Global indicators of X-ray data quality. J. Appl. Crystallogr. *34*, 130–135.

Wigley, D.B., Davies, G.J., Dodson, E.J., Maxwell, A., and Dodson, G. (1991). Crystal structure of an N-terminal fragment of the DNA gyrase B protein. Nature *351*, 624–629.

Winn, M.D., Ashton, A.W., Briggs, P.J., Ballard, C.C., and Patel, P. (2002). Ongoing developments in CCP4 for high-throughput structure determination. Acta Crystallogr. D Biol. Crystallogr. *58*, 1929–1936.

Winn, M.D., Isupov, M.N., and Murshudov, G.N. (2001). Use of TLS parameters to model anisotropic displacements in macromolecular refinement. Acta Crystallogr. D Biol. Crystallogr. *57*, 122–133.

Xu, Z., Bernlohr, D.A., and Banaszak, L.J. (1993). The adipocyte lipid-binding protein at 1.6-A resolution. Crystal structures of the apoprotein and with bound saturated and unsaturated fatty acids. J. Biol. Chem. *268*, 7874–7884.

Yoon, M.Y., and Cook, P.F. (1987). Chemical mechanism of the adenosine cyclic 3′,5′-monophosphate dependent protein kinase from pH studies. Biochemistry *26*, 4118–4125.

Zanotti, G., Scapin, G., Spadon, P., Veerkamp, J.H., and Sacchettini, J.C. (1992). Three-dimensional structure of recombinant human muscle fatty acid-binding protein. J. Biol. Chem. *267*, 18541–18550.

Zhang, C.C. (1996). Bacterial signalling involving eukaryotic-type protein kinases. Mol. Microbiol. *20*, 9–15.

Zhang, W., and Shi, L. (2004). Evolution of the PPM-family protein phosphatases in Streptomyces: duplication of catalytic domain and lateral recruitment of additional sensory domains. Microbiology *150*, 4189–4197.